Spectral POD Analysis of Dual Vortex Shedding Modes Around Intermediate Rectangular Cylinders

Sedem Kumahor
Department of Mechanical Engineering
University of Manitoba
Winnipeg, Manitoba, R3T 5V6, Canada
kumahors@myumanitoba.ca

Xingjun Fang
Institute of Mechanics
Chinese Academy of Sciences
Beijing, PR China
fangxj@imech.ac.cn

Robert J. Martinuzzi
Department of Mechanical and Manufacturing Engineering
University of Calgary
Calgary, Alberta, T2N 1N4, Canada
rmartinu@ucalgary.ca

Mark F. Tachie
Department of Mechanical Engineering
University of Manitoba
Winnipeg, Manitoba, R3T 5V6, Canada
mark.tachie@umanitoba.ca

ABSTRACT

Turbulent flows around two-dimensional rectangular cylinders with intermediate streamwise aspect ratios of AR = 2 and 2.5 were experimentally studied using time-resolved particle image velocimetry (TR-PIV) at a Reynolds number (based on free-stream velocity and cylinder height) of 16200. These aspect ratios represent a transition from direct shear layer shedding into the wake (AR < 2) and mean reattachment on the cylinder (AR > 3.5). For these transitional aspect ratios, an uncharacteristically large wake vortex occurs together with a dual-shedding vortex mechanism that is still poorly understood. Spectral proper orthogonal decomposition (SPOD) is applied to the TR-PIV data to educe the spatiotemporal dynamics of coherent structures at the various shedding frequencies. Results evidence a dual shedding frequency phenomenon from the spectra of the fluctuating velocities, reverse flow area and SPOD. Specifically, the lower frequency ($St = 0.084$) is dominant over $St = 0.142$ for AR=2, while the higher frequency ($St = 0.150$) is dominant over $St = 0.056$ for AR=2.5. Regardless of AR, SPOD reconstruction reveals that the lower or higher frequencies capture similar vortex shedding patterns.

INTRODUCTION

Flow around rectangular cylinders in a uniform stream is a canonical geometry used to investigate separated flows and vortex shedding characteristics (Nakagawa et al., 1999; Knisely, 1990; Mohebi et al., 2017; Moore et al., 2019). Above a critical Reynolds number of 150 (Franke et al., 1990; Mashhadi et al., 2021), the flow separates at the sharp leading edge. The shear layer reattaches on the cylinder if the streamwise aspect ratio (AR $= L/h$, where L is streamwise length and h is the cylinder height) is larger than 3.5. The reattached flow subsequently separates at the trailing edge and wake periodicity is observed to be coupled with the shear layer instabilities. For low aspect ratios (AR < 2.0) (Nakagawa et al., 1999; Knisely, 1990; Mohebi et al., 2017; Moore et al., 2019), the shear layer extends into the wake and a direct coupling through the Kármán process gives rise to periodic vortex shedding. For intermediate aspect ratios (2 < AR < 3.5), transition from direct shear layer shedding in the wake and reattachment regimes occur. This regime is characterized by the formation of a large wake recirculation region and the occurrence of dual vortex shedding mechanism (Okajima, 1982; Knisely, 1990; Nakagawa et al., 1999; Kumahor and Tachie, 2023). While the mean flow topology and the dual vortex shedding frequencies are well documented for intermediate aspect ratios, the underlying formation mechanisms and dynamics of the coherent structures formed at these frequencies remain poorly understood.

Briefly, previous investigations for intermediate aspect ratios studied the mean flow structure or temporal flow characteristics using frequency spectra analysis. Their results show an uncharacteristically large wake vortex and spectral energy concentrated at two frequencies often denoted as dual vortex shedding frequencies (Okajima, 1982; Knisely, 1990; Nakagawa et al., 1999; Kumahor and Tachie, 2023; Liu et al., 2024). For AR=2, a low frequency ($St = fh/U_e = 0.08$, is the Strouhal number based on the spectral-peak frequency f and free-stream velocity U_e) was reported to be dominant over a high frequency $St = 0.15$ (Okajima, 1982; Knisely, 1990; Kumahor and Tachie, 2023). To the best of the authors' knowledge, there are no studies on the AR=2.5 cylinder.

Proper orthogonal decomposition (POD) is a spatio-temporal analysis (gives time and spatial modes) that has been applied to extract coherent structures from TR-PIV data for rectangular cylinders with varying AR in uniform flow (Mohebi et al., 2017; Kumahor and Tachie, 2023). The results showed that when there is regular vortex shedding patterns, the first mode pair contained similar energy content, a phase portrait of their mode coefficients exhibited circular patterns and a single dominant frequency peak was observed. Meanwhile, for the AR=2 cylinder, significant cycle-to-cycle variation was observed in the phase portrait due to the irregular vortex shedding patterns and dual vortex shedding frequencies were observed (Okajima, 1982; Norberg, 1993; Kumahor and Tachie, 2023).

Spectral proper orthogonal decomposition (SPOD) is an analysis tool that is garnering popularity in the turbulence community (Towne et al., 2018; Fang et al., 2022; Chen et al., 2023). SPOD utilizes time-resolved data to resolve coherent structures spatially and in the frequency domain. The key difference between POD and SPOD is that the fluctuating velocity field is decomposed into different modes at different frequencies in the implementation of SPOD, enabling the extraction of dominant coherent structures occurring at specific shedding frequencies (Towne et al., 2018). In principle, this method allows the characterization of coherent structures at any dynamically important (i.e., high fluctuation energy concentration) frequency, and therefore provides a unique opportunity to elucidate the underlying dynamics of the dual vortex shedding motions.
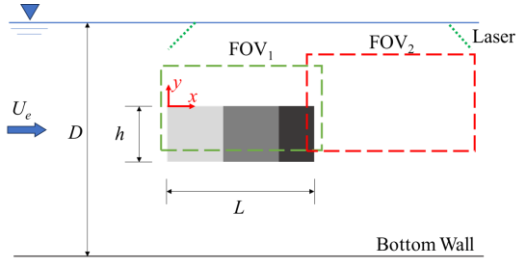
Figure 1: Schematic (not to scale) of the experimental setup, fields of view, nomenclature and coordinate system adopted.

The objective of the present study is to apply SPOD on the separating flows around intermediate rectangular cylinders of AR=2 and 2.5. The square cylinder, which is the most studied rectangular cylinder with AR=1 is also investigated as a reference case for regular (von-Kármán) vortex shedding.

EXPERIMENTAL SET-UP

The experiments were performed in an open recirculating water channel at the Turbulence and Hydraulic Engineering Laboratory (THEL) at the University of Manitoba. Figure 1 illustrates the side view of the test section along with the fields of view (FOV), nomenclature and coordinate system adopted in this study. The streamwise length, spanwise width and vertical height of the test section are 6000 mm, 600 mm and 450 mm, respectively. Three rectangular cylinders with fixed vertical height, h = 30 mm and spanwise width, B = 580 mm were machined from smooth acrylic plates, with streamwise lengths (L) of 30 mm (AR=1), 60 mm (AR=2) and 75 mm (AR=2.5). The water depth (D) was kept constant at 430 mm and the cylinders were horizontally positioned such that the cylinder mid-height was 215 mm above the bottom wall and spanned the channel width. The free-stream velocity was set to U_e = 0.54 m/s so that Reynolds number based on cylinder height and free-stream velocity was 16200. The turbulence intensity measured at the channel mid-height in the absence of the cylinder was 1.2%. The origins of the streamwise (x) and vertical (y) coordinates are set at the leading edge and top surface of the cylinder, respectively.

Time-resolved particle image velocimetry was used to perform velocity measurements at the mid-span of the channel. The water was seeded with 10 μm silver coated hollow glass spheres with a nominal density of 1400 kg/m^3. A diode pumped dual-cavity high-speed Neodymium-doped yttrium lithium fluoride laser (*Photonics Industries* DM30-527DH) with maximum pulse energy of 30 mJ/pulse for each cavity was used to illuminate the seeding particles. Two high speed 12-bit CMOS cameras (*Phantom* VEO 340L) of resolution, 2560 pixel × 1600 pixel positioned side-by-side were used to simultaneously image the seeding particles in two fields-of-view. The dimensions of the FOVs over the cylinders and wake region were, respectively, $3.3h \times 2.1h$ and $4.6h \times 2.9h$, resulting in scaling factors of 25.0 pixel/mm and 18.4 pixel/mm, respectively. Since the mean flow is symmetric about the cylinder centerline, only the upper half was captured to maximize the spatial resolution of the cameras. The sampling frequency was set to 800 Hz and 96000 images were captured for each test case, resulting in 120 seconds of sampling time. Data acquisition and image post-processing were performed using commercial software (DaVis 10.0.5) supplied by *LaVision Inc*. Velocity vectors were calculated using a GPU-accelerated multi-pass cross-
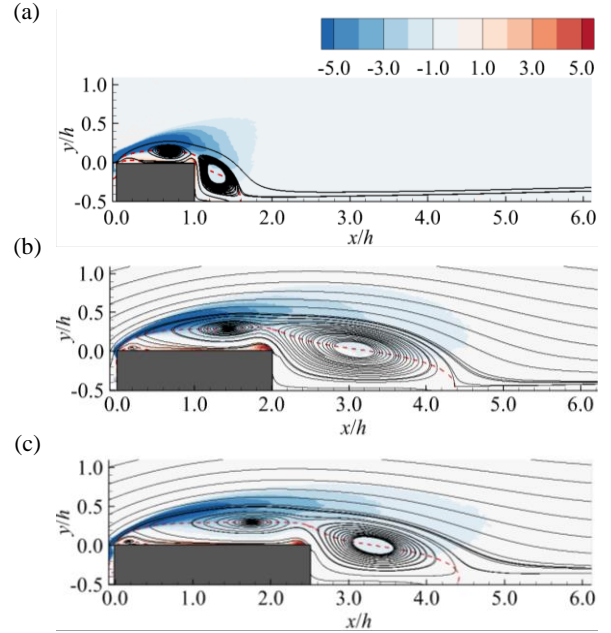

Figure 2: Mean streamwise vorticity, superimposed with the mean streamlines (continuous lines) and the isopleth of U = 0 (red dashed lines) for AR=1 (a), AR=2 (b) and AR=2.5 (c).

correlation algorithm with a single initial pass of 128 pixel × 128 pixel interrogation area (IA) with 50% overlap, followed by four final passes of 24 pixel × 24 pixel IA with 75% overlap. The vector spacing was 0.20 mm (0.007h) and 0.33 mm (0.011h) for FOVs over the cylinders and in the wake region, respectively. The worst-case measurement uncertainties at 95% confidence level were 2.6% and 6.9% in the mean velocities and Reynolds stresses, respectively, at the location of maximum $(\overline{u'u'})$ for AR=1, due to exceptionally high local turbulence levels (Kumahor and Tachie, 2023).

RESULTS AND DISCUSSION

Figure 2 shows contours of the mean spanwise vorticity, superimposed with the mean streamlines and isopleths of U = 0 (dashed lines). For all aspect ratios, vorticity is concentrated at the leading edge and diffuses into wider bands as the wake is approached, illustrating the trajectory of the separated shear layer. The separated shear layer extends directly into the wake region for all tested aspect ratios and the primary and wake recirculation bubbles over and behind the cylinders, respectively, are dynamically coupled. The recirculation lengths, which were determined as the streamwise distance between the trailing face of the cylinders to the location of U = 0 along the symmetry plane, are x_L/h = 0.60, 2.40 and 1.90, respectively, for AR=1, AR=2 and AR=2.5. The recirculation length for AR=1 is consistent with the results of Trias et al (2015) and Mohebi et al. (2017). For AR=2, Nakagawa et al. (1999) reported x_L/h = 1.8, which is 25% shorter than the present value, and is likely due to a higher oncoming turbulence intensity (6%) and blockage ratio (20%), which promote early deflection of the shear layer into the wake region. Near the leading edge, a small recirculation bubble is formed due to the adverse pressure gradient formed by the upstream flowing fluid along the cylinder surface. The secondary recirculation bubble counter-rotates with respect to the primary bubble as evidenced in the region of positive vorticity near the leading edge.
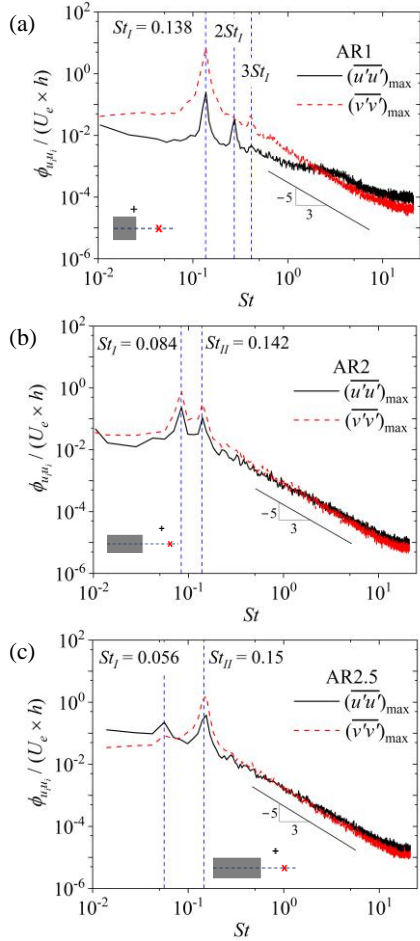
Figure 3: Frequency spectra of the streamwise (ϕ_{uu}) and vertical (ϕ_{vv}) fluctuating velocity at locations of maximum $\overline{(u'u')}$ and $\overline{(v'v')}$, respectively for AR 1 (a), AR=2 (b) and AR=2.5 (c). Inserts show the relative locations of maximum $\overline{(u'u')}$ (+) and maximum $\overline{(v'v')}$ ($\times$)

Consistent with Moore et al. (2019) for rectangular cylinders without mean reattachment, an upward bump at the trailing edge is seen in the mean streamlines and characterized by positive vorticity in this region. This occurrence is a consequence of the reverse flow in the wake impinging on the trailing face and separating at the trailing edge, before flowing upstream over the cylinder. The magnitude of the vorticity near the trailing edge is highest for AR=2 and lowest for AR=1. Furthermore, the magnitude of reverse flow (although not shown) is highest for AR=2, generating stronger upwash and higher bump at the trailing edge, which significantly alters the trajectory of the descending separated shear layer, leading to its streamwise elongation and resultant large wake recirculation bubble.

Figure 3 shows the frequency spectra of the streamwise and vertical fluctuating velocities at the locations of maximum $\overline{(u'u')}$ and $\overline{(v'v')}$, respectively. A dominant peak at a Strouhal number corresponding to the fundamental von-Kármán shedding frequency for AR=1 is observed ($St = 0.138$) together with higher harmonics, which is in good agreement with prior studies (Okajima, 1982; Mohebi et al., 2017). For AR=2 and AR=2.5, in contrast, dual peaks which are not integer multiples of each other are evident. Consistent with
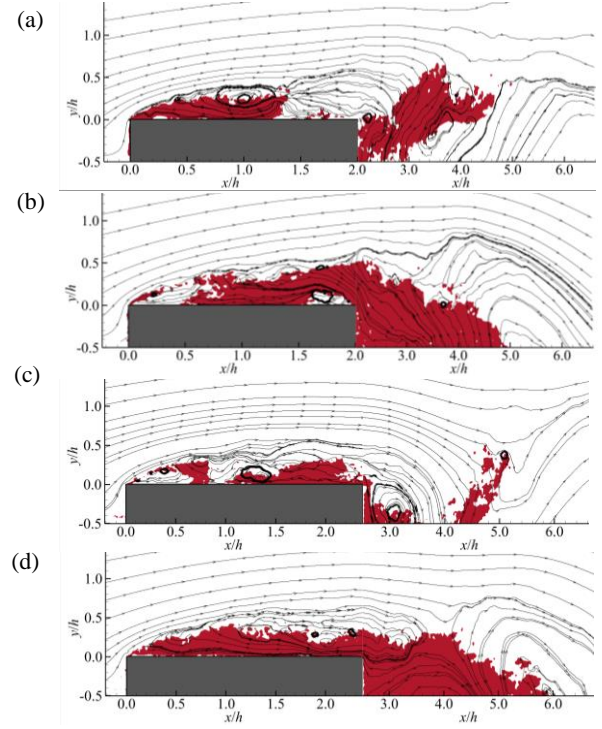

Figure 4: Typical instantaneous contours of the reverse flow area ($u < 0$) superimposed with the instantaneous streamlines for AR=2 (a,b) and AR=2.5 (c,d).

Okajima (1982), Knisely, (1990) and Norberg (1993), peaks at $St = 0.084$ and 0.142 are observed for AR=2 with $St = 0.084$ being dominant. For AR=2.5, $St = 0.150$ dominates over $St = 0.056$.

The instantaneous expansion and contraction of the recirculation region, typically observed as the flapping of the shear layer which bounds the recirculation region, are observed around the cylinders and visualized using the reverse flow area and instantaneous streamlines in Figure 4. Following Pearson et al. (2013) and Fang and Tachie (2019), the instantaneous reverse flow area is used to measure the size of the instantaneous separation bubble, which is calculated by summing up the areas of $u < 0$ within a region of interest. The analysis is restricted to $x/h \times y/h \in [-0.5, 6.0] \times [-0.5, 1.6]$ and excluding the area identified as the cylinder. The mean reverse flow area was $\bar{A}/h^2 = 0.54, 1.53, 1.72$ for AR=1, 2 and 2.5, respectively, signifying the larger recirculating regions for the intermediate cylinders, compared to AR=1. For brevity, only the visualizations for AR=2 and 2.5, are presented in Figure 4.

Figures 4(a) and 4(b), respectively, show typical instances of instantaneous reattachment onto the AR=2 cylinder and direct shedding into the wake. The contrast in the recirculation region is immediately apparent. On flow reattachment, the size of the wake recirculation region is considerably smaller, and the streamlines show separation at the trailing edge. During direct shedding (Figure 4(b)), the upwash of reversing fluid is observed near the trailing edge and is signified by the upward bump and recirculation bubble. The wake recirculation region is much larger, and the streamlines emanating from the leading edge descend further downstream. Careful examination of many instantaneous snapshots shows that this state of direct shedding occurs more frequently, resulting in the large wake recirculation region.
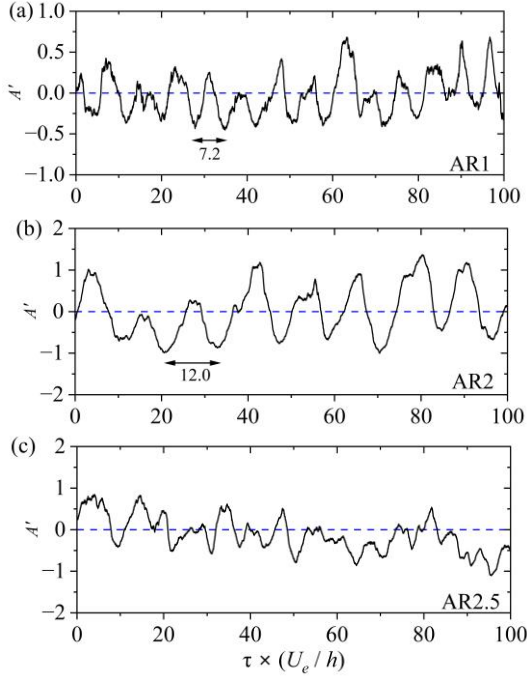
Figure 6: Time history of the fluctuating reverse flow area for AR=1 (a), AR=2 (b) and AR=2.5 (c).
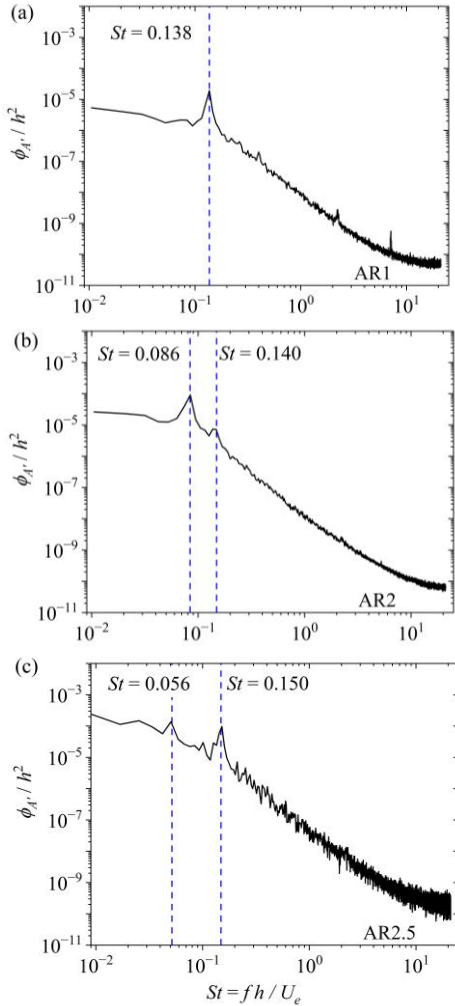

Figure 7: Frequency spectrum of the fluctuating reverse flow area ($\phi_{A'}$) for AR=1 (a), AR=2 (b) and AR=2.5 (c).

For AR=2.5, typical instances of reattachment and direct shedding are shown in Figures 4(c) and (d), respectively. Instantaneous reattachment occurs closer to the leading edge compared to AR=2, while a larger and continuous recirculation region is observed during direct shedding into the wake. This observation is consistent with the larger mean reverse area for AR=2.5 compared to AR=2. Near the trailing edge, the upwash of reversing fluid is less prominent, alluding to the smaller recirculation length measured from the trailing edge ($x_L/h = 1.90$) compared to AR=2 ($x_L/h = 2.40$).

To assess the expansion and contraction of separation bubbles, the time history and frequency spectra of the fluctuating reverse flow area ($A' = A - \bar{A}$) are presented in Figures 6 and 7, respectively. The time history shows quasi-periodic enlargement and contraction of the reverse flow region, which is reminiscent of the flapping motions of separation bubbles observed by Kiya and Sasaki (1983), Castro and Haque (1987) and Fang et al., (2022). The non-dimensional period between successive troughs or crests for AR=1 and AR=2 relate to the inverse of the dominant Strouhal number ($St = 0.138$ and 0.084, respectively), due to their higher spectral energy. For AR=2.5, the dual frequencies contain comparable spectral energy (Figure 7(c)), thus the time history shows a beating pattern that is indicative of the co-dominance of vortex shedding occurring at both frequencies.

While previous studies on the AR=2 cylinder investigated the dual peaks using point-wise measurement techniques (Okajima, 1982; Knisely, 1990; Norberg, 1993), for the first time, a whole-field technique is used to verify these results. The results of the frequency spectra analysis using the fluctuating reverse flow area are consistent with those from fluctuating velocity signals. A single dominant peak is observed for AR=1, while dual peaks are observed for AR=2 and 2.5. This indicates that the dual shedding patterns are supported by sufficiently large spatial structures to alter the size of the entire separation bubble and the reverse flow area is a suitable technique to capture vortex shedding dynamics.

To identify the structures underlying the oscillations of the separation bubble, SPOD analysis is performed for the same region of interest as the reverse flow area. Figure 8 shows the premultiplied frequency spectra of the first two SPOD mode pairs. The frequency peaks captured in the SPOD modes are identical to those shown in Figures 3 and 7 using the fluctuating velocities and reverse flow area. The dominant peaks for AR=2 and 2.5 are also consistent. In general, the spectral energy captured within the first mode pair is at least an order of magnitude higher than the second mode pair, regardless of aspect ratio.

The spatial modes at the two highest peaks for each test case are compared in Figure 9. As shown in Figure 9(a) for AR=1, the alternating patterns at $St = 0.138$ capture the von-Kármán vortex shedding patterns and the vortex centers are located along the symmetry plane. The second harmonic ($St = 0.276$) in Figure 9(d) captures smaller wavelength structures that are off-centered from the symmetry plane. For AR=2 and AR=2.5, the lower frequencies (Figure 9(b,c)) capture a long wavelength structure that emanates from the leading edge and is extended into the wake, with the vortex cores centered on the symmetry plane. Meanwhile, the higher frequencies capture shorter wavelength structures that emanate from the trailing edge but, unlike AR=1, their vortex cores are centered on the symmetry plane. For AR=2, $St = 0.084$ dominates over $St = 0.142$ suggesting that the dominant structures emanate
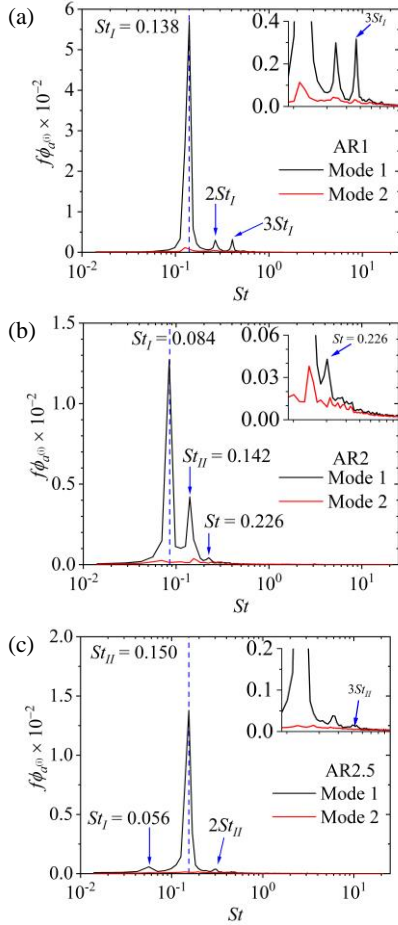
Figure 8: Premultiplied frequency spectra of the first and second SPOD modes for AR=1 (a), AR=2 (b) and AR=2.5 (c).

from the leading edge and extend directly into the wake, corroborating the longer recirculation length. For AR=2.5, $St = 0.150$ dominates and the shorter wavelength structures act to result in a short recirculation length.

Low-order reconstruction of typical instantaneous vorticity flow fields using the first SPOD mode pair at the dominant frequencies are presented in Figure 10 for AR=2 and 2.5. The lower frequencies for AR=2 and 2.5 (row 1 and 3) show similar vortex shedding patterns. Specifically, the vorticity in the shear layer appears in two opposing bands, changing signs as the vortex formation process progresses. Meanwhile, the higher frequencies at both aspect ratios (row 2 and 4) show a single band of vorticity which does not change sign over the cylinder. Furthermore, the streamlines show that instantaneous reattachment over the cylinder is more prominent at the higher frequencies for both aspect ratios. These observations suggest that, regardless of aspect ratio, the lower or higher frequencies capture similar vortex formation processes and their co-interaction give rise to the dual shedding frequency phenomenon.

SUMMARY AND CONCLUSION

In this study, turbulent flows around intermediate rectangular cylinders with streamwise aspect ratios of AR=2 and 2.5 were experimentally studied using time-resolved particle image velocimetry (TR-PIV) at a Reynolds number of 16200 and the results were compared to a square cylinder at the same Reynolds number. These aspect ratios are

particularly interesting as they mark the transition from direct shear layer shedding into the wake (AR < 2) and mean reattachment onto the cylinder (AR > 3.5) occur. The observed flow behavior for these aspect ratios revealed an unusual phenomenon characterized by an exceptionally large wake vortex coupled with a dual-shedding vortex mechanism.

Analysis of the mean flow topology revealed a significantly larger wake region for AR=2 and 2.5 compared to AR=1. The recirculation length measured from the trailing edge was found to be $x_L/h = 2.40$ for AR=2 and 1.90 for AR=2.5, despite the larger mean reverse flow area observed for A=2.5. This discrepancy in recirculation wake length is attributed to the strong upwash of reversing flow near the trailing edge for AR=2.

Frequency spectra of the fluctuating velocities and reverse flow area show a dual shedding frequency phenomenon for AR=2 and AR=2.5. To unravel the spatiotemporal dynamics of coherent structures at these various shedding frequencies, Spectral Proper Orthogonal Decomposition (SPOD) was applied to the TR-PIV data. Consistent with the fluctuating velocities and reverse flow area, the results also show a dual shedding frequency phenomenon. Specifically, the lower frequency ($St = 0.084$) is dominant over $St = 0.142$ for AR=2, while the higher frequency ($St = 0.150$) is dominant over $St = 0.056$ for AR=2.5. Regardless of AR, SPOD reconstruction reveals that the lower or higher frequencies capture similar vortex shedding patterns.

REFERENCES

Castro, I. P., and Haque, A., 1987, "The structure of a turbulent shear layer bounding a separation region", *Journal of Fluid Mechanics*, Vol. 179, pp. 439-468.

Chen, G., Li, X., Xue, R., He, K., Wang, H., and Liang, X., 2023, "Effects of incoming free-stream turbulence on the flow dynamics of a square finite wall-mounted cylinder", *Physics of Fluids*, Vol. 35, 025140.

Fang, X., and Tachie, M. F., 2019, "On the unsteady characteristics of turbulent separations over a forward-backward-facing step", *Journal of Fluid Mechanics*, Vol. 863, pp. 994-1030.

Fang, X., Tachie, M. F., and Dow, K., 2022, "Turbulent separations beneath semi-submerged bluff bodies with smooth and rough undersurfaces", *Journal of Fluid Mechanics*, Vol. 947, A19.

Franke, R., Rodi, W., and SchÖnung, B., 1990, "Numerical calculation of laminar vortex-shedding flow past cylinders", *Journal of Wind Engineering and Industrial Aerodynamics*, Vol. 35, pp. 237–257.

Knisely, C. W., 1990, "Strouhal numbers of rectangular cylinders at incidence: a review and new data", *Journal of Fluids and Structures*, Vol. 4, pp. 371-393.

Kiya, M. and Sasaki, K., 1983, "Structure of a turbulent separation bubble", *Journal of Fluid Mechanics*, Vol. 137, pp. 83-113.

Kumahor, S., and Tachie, M. F., 2023, "Effects of streamwise aspect ratio on the spatio-temporal characteristics of flow around rectangular cylinders", *International. Journal of Heat and Fluid Flow*, Vol. 101, 109133.

Liu, M., Kumahor, S., and Tachie, M. F., 2024, "Reynolds number effects on turbulent wakes generated by rectangular cylinders with streamwise aspect ratios between 1 and 4", *Journal of Fluids Engineering*, Vol. 146, 021303.
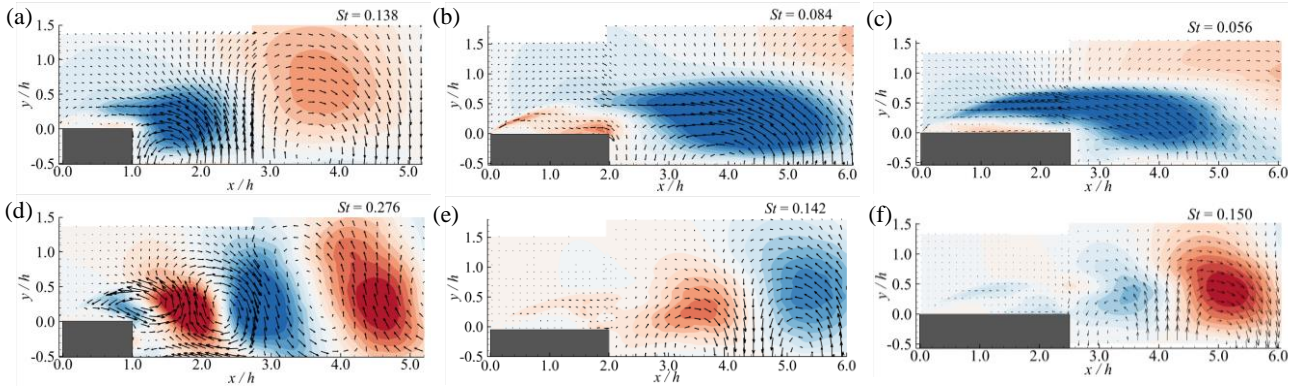
Figure 9: The first SPOD mode at the frequency peaks for AR=1 (a,d), AR=2 (b,e) and AR=2.5 (c,d). The Strouhal number is indicated at the top right corner on each figure. Animated version will be presented.
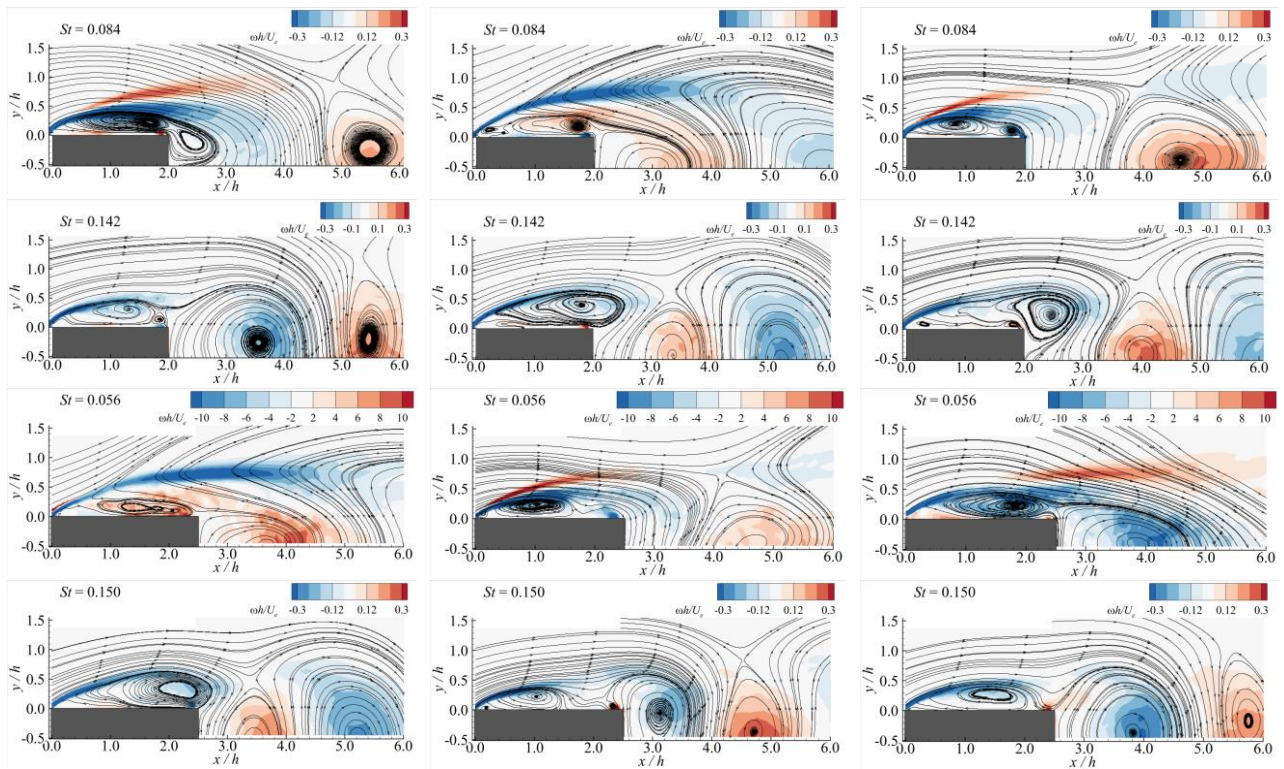

Figure 10: SPOD reconstruction of the instantaneous spanwise vorticity (ω) using the first mode pair at the frequency peaks for AR=2 (first two rows) and AR=2.5 (bottom two rows)

Mashhadi, A., Sohankar, A., and Alam, M. M., 2021, "Flow over rectangular cylinder: Effects of cylinder aspect ratio and Reynolds number", *International Journal of Mechanical Sciences*, Vol. 195, 106264.

Mohebi, M., Plessix, P., Martinuzzi, R. J., and Wood, D. H., 2017, "Effect of thickness-to-chord ratio on the wake of two-dimensional rectangular cylinders", *Physical Review Fluids*, Vol. 2, pp. 064702.

Moore, D. M., Letchford, C. W., and Amitay, M., 2019, "Energetic scales in a bluff body shear layer." *Journal of Fluid Mechanics*, Vol. 875, pp. 543-575.

Nakagawa, S., Nitta, K., and Senda, M., 1999, "An experimental study on unsteady turbulent near wake of a rectangular cylinder in a channel flow." *Experiments in Fluids*, Vol. 27, pp. 284–294.

Norberg, C., 1993, "Flow around rectangular cylinders: Pressure forced and wake frequencies", *Journal. of Wind Eng. and Industrial Aerodynamics*, Vol. 49, pp. 187–196.

Okajima, A., 1982, "Strouhal numbers of rectangular cylinders", *Journal of Fluid Mechanics*, Vol. 123, pp. 379–398.

Otsuki, Y., Washizu, K., Tomizawa, H., and Ohya, A., 1974, "A note on the aeroelastic instability of a prismatic bar with square section." *Journal of Sound and Vibration*, Vol. 34, pp. 233-248.

Pearson, D. S., Goulart, P. J., and Ganapathisubramani, B., 2013, "Turbulent separation upstream of a forward-facing step", *Journal of Fluid Mechanics*, Vol. 724, pp. 284-304.

Towne, A., Schmidt, O. T., and Colonius, T., 2018, "Spectral proper orthogonal decomposition and its relationship to dynamic mode decomposition and resolvent analysis", *Journal of Fluid Mechanics,* Vol. 847, pp. 821–867.

Trias, F., Gorobets, A., and Olivia, A., 2015, "Turbulent flow around a square cylinder at Reynolds number 22,000: A DNS study", *Computers and Fluids*, Vol. 123, pp. 87-98.